



HAL
open science

Microstructural characterization of NiAl–Al₂O₃ composite materials obtained by in situ aluminothermic reduction of NiO for potential coating applications

R. Troncy, Gilles Bonnet, F. Pedraza

► **To cite this version:**

R. Troncy, Gilles Bonnet, F. Pedraza. Microstructural characterization of NiAl–Al₂O₃ composite materials obtained by in situ aluminothermic reduction of NiO for potential coating applications. *Materials Chemistry and Physics*, 2020, 251, pp.123124 -. 10.1016/j.matchemphys.2020.123124 . hal-03491558

HAL Id: hal-03491558

<https://hal.science/hal-03491558>

Submitted on 18 Jul 2022

HAL is a multi-disciplinary open access archive for the deposit and dissemination of scientific research documents, whether they are published or not. The documents may come from teaching and research institutions in France or abroad, or from public or private research centers.

L'archive ouverte pluridisciplinaire **HAL**, est destinée au dépôt et à la diffusion de documents scientifiques de niveau recherche, publiés ou non, émanant des établissements d'enseignement et de recherche français ou étrangers, des laboratoires publics ou privés.



Distributed under a Creative Commons Attribution - NonCommercial 4.0 International License

Microstructural characterization of NiAl-Al₂O₃ composite materials obtained by in situ aluminothermic reduction of NiO for potential coating applications

R. Troncy^{1, a}, G. Bonnet^{1, b}, F. Pedraza^{1, c}

¹ La Rochelle Université. LaSIE, UMR-7356-CNRS. Avenue Michel Crépeau, 17042 La Rochelle Cedex 1, France

^aromain.troncy1@univ-lr.fr, ^bgbonnet@univ-lr.fr, ^cfpedraza@univ-lr.fr

Abstract

Aluminothermic reactions between Al microparticles and preoxidized Ni particles were carried out to fabricate mixed compounds of Ni_xAl_y containing in situ generated Al₂O₃. The mixed composites were obtained by applying a thermal treatment to either a mixture of NiO and Al powders or to a stacking of powders. The effects of the particle size, thickness of oxide, heating ramp and temperature on the microstructure of the NiAl-Al₂O₃ coating are discussed. The results indicate that Ni₃Al forms first during the synthesis, followed by NiAl and Al₃Ni₂ while Al₃Ni forms on cooling. Moreover, the alumina was observed to form a continuous network surrounding Ni_xAl_y intermetallic compounds. It derives that these composites have a potential to form self-healing coatings.

1. Introduction

Nowadays, the demand for materials with high performances at elevated temperature is in constant increase. Nickel based superalloys possess excellent mechanical properties at high temperature due to their high melting point. However, their resistance to oxidation by hot gases and to so-called hot corrosion appears limited [1, 2]. To overcome these disadvantages, the use of intermetallic compounds was developed. NiAl is the most attractive due to capacity to develop a protective aluminum oxide layer through oxidation [3, 4]. The coating acts as an aluminum reservoir whereby aluminum is consumed by oxidation at the surface of the coating to form an alumina protective layer [1, 2, 5, 6]. Further, Al diffuses into the substrate, which lowers the overall Al content in the coating. Below a critical concentration, other non-protective oxides such as NiAl₂O₄ and NiO may form resulting in the rapid degradation of the material. For instance, during the oxidation of Ni(Pt)Al systems at high temperature (100 h at 1050°C), 2 to 8% of Al are consumed by the formation of the aluminum oxide while 20 to 35% of Al are “lost” by diffusion to the superalloy substrate [7]. Diffusion barriers can be employed to prevent diffusion of aluminum in the substrate. These diffusion barriers can be made of refractory elements or rare-earth ones whose effectiveness to slow down the diffusion of aluminum has been demonstrated [8-10]. However, such diffusion barriers mechanically weaken the coated components and increase the coating prices.

Our approach to maintain a sufficient amount of Al is to introduce aluminum micro-containers into the coating so that Al is released once a concentration gradient is established between the reservoir and the Al-impooverished coating matrix. The micro-containers are small volumes (tens of μm) of an Al-rich Ni_xAl_y intermetallics compound entrapped by aluminum oxide. The micro-containers shall thus have an Al-rich intermetallic core (Al₃Ni or Al₃Ni₂) encapsulated in an alumina shell. The intermetallic core can be synthesized by Self Propagating High-Temperature Synthesis (SHS). SHS is a complex thermally activated

physicochemical process that takes place at elevated temperatures [11]. A great number of factors and process conditions can exert a significant influence on the results, in particular temperature, time, size of the particles, heating and cooling rates, pressure and atmosphere [12, 13]. The relationship between these different parameters and the reaction process between the three elements (Ni, Al and O) was reported by Levin & al. and results in multiphase (metal, liquid and oxide) components as shown in Fig. 1 [14].

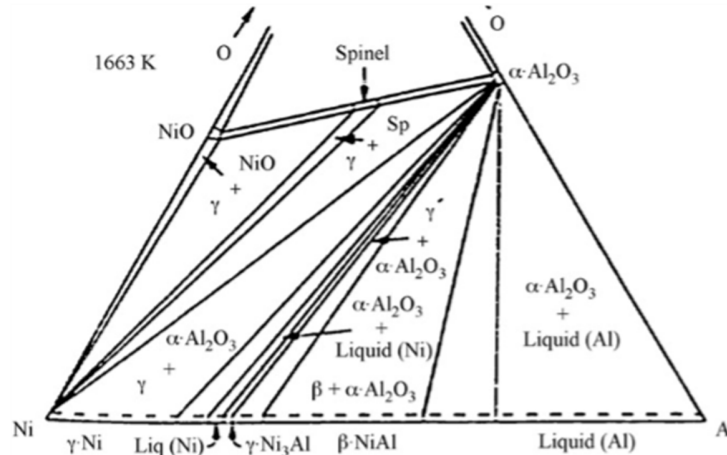
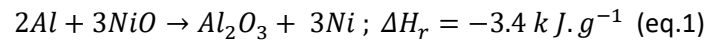


Fig. 1: Ternary phase diagram of Ni-Al-O at 1638 K (1365°C) [14].

The alumina shell can be produced in situ by an aluminothermic process following the thermite reaction (eq. 1) [15]:



The redox reaction between NiO and Al results in the release of a large amount of energy. The products of such a reaction are solid, liquid and sometimes gaseous, inducing an intense sputtering and destruction of the samples [16, 17]. However, the exothermic effect can be inhibited by the addition of an inert diluent, i.e. of a heat absorber. Vrel et al. studied the effects of the addition of alumina and of the limitation of one of the two reagents on the aluminothermic reaction [16, 17]. In addition, Biswas et al. [18] reported that the heating rate and the particle size could be modified to limit the amount of energy released and produce different intermetallic compounds. For instance, low heating rates and a large size of particles can cancel the explosion of the powders.

Based on the above, the Al-Ni SHS and the aluminothermic reactions will be combined in this work to synthesize $Ni_xAl_y-Al_2O_3$ phases that could serve as self-healing coatings. Different parameters including particle size, heating rates, amount of nickel oxide and contact area between particles will be studied.

2. Experimental procedure

Commercially available Ni microparticles underwent a preoxidation treatment at 700°C in air for different times to form NiO oxide shells over the Ni powders. This oxidation temperature of 700°C was chosen following the works of Peraldi et al. [19, 20], who described the microstructure of the oxide scales grown on pure Ni as function of temperature and time. The porous NiO formed at 700°C for short

times is expected to facilitate the Al flow during the SHS reactions. The particles size of the powders and the time of preoxidation are given in Table 1.

Table 1: Main features of initial Ni, Al and preoxidized Ni particles.

Powder	Aluminum	Nickel 1	Nickel 2	Nickel 1 preoxidized	Nickel 1 preoxidized	Nickel 2 preoxidized	Nickel 2 preoxidized
Symbol	Al	Ni-1	Ni-2	Ni-1.a	Ni-1.b	Ni-2.a	Ni-2.b
Purity (wt %)	99.8	99.95	99.9	---	---	---	---
Size (μm)	4 \pm 3	31 \pm 19	11 \pm 6	10 \pm 9	17 \pm 14	7 \pm 4	5 \pm 3
Morphology	Spherical	Spherical	Pseudo-spherical	Pseudo-spherical	Pseudo-spherical	Pseudo-spherical	Pseudo-spherical
Oxidation time at 700°C	0	0	0	1 h	4 \times 1 h	3 \times 5 min	4 \times 10 min
Supplier	Hermillon	GoodFellow	Alfa Aesar	---	---	---	---

The coarse powder (Ni-1) was heated at 700°C for 1h (Ni-1.a) and 4h (Ni-1.b) in air (intermediate crushing in a mortar every hour). The small-sized powder (Ni-2) underwent the same preparation but the oxidation time was of 15 min (Ni-2.a) and 40 min (Ni-2.b) (intermediate crushing every 5 and 10 min, respectively). The intermediate crushing step was realized to increase the oxide thickness and avoid sintering. Such partial oxidation is assumed to present two simultaneous advantages, i.e. to reduce the energy release during the thermite reaction and to lower the content of one of the two reagents like in the works of Vrel et al. [16, 17]. Moreover, it allows to keep a metal core surrounded by a porous NiO to form the desired composite compounds [18-20].

A powder mixture containing the preoxidized nickel particles and aluminum particles was blended in the stoichiometric atomic ratio to form NiAl according to the Al-Ni binary diagram (Fig. 2.a). In addition, the preoxidized nickel particles were deposited over the Al microparticles (Fig. 2.b) to simulate the interfacial reactions of a potential coating. Both configurations (mixed and stacked powders) were placed in alumina crucibles for the DSC experiments (SETARAM Labsys Evo 1600 thermal analysis). The heating rates were fixed at 2 and 25°C/min with a maximum temperature of 1300°C; the cooling rate was fixed at 50°C/min (to keep the microstructures and crystal phases obtained at high temperature). Upon annealing, the reaction chamber was ventilated with a flow of Ar (20 mL/min) to limit oxidation phenomena and prevent secondary reactions in the system, although some air can be trapped between the powders when poured into the crucible. For each test, energy changes and reaction temperatures were determined using the Calisto software coupled to the DSC technique. To identify all the transformations, additional heat treatments were performed in the same conditions but the tests were interrupted at 750 and 1000°C.

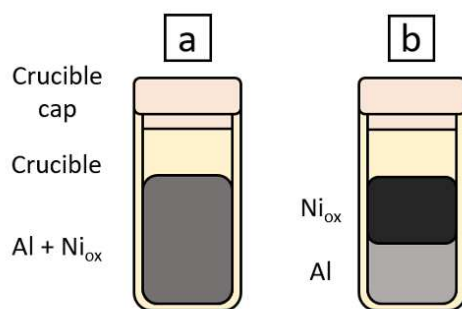


Fig. 2: Schematic drawings representing the two different layouts: (a) mixture of preoxidized Ni and of Al particles; (b) preoxidized Ni over the Al particles.

After the heat treatment, the crucibles were prepared for microscopy observation of the cross-sections. They were thus mounted in a phenolic resin, ground till SiC P4000 and finally polished with a 1 μm diamond suspension (Struers). The characterization of the cross-sections was performed with a SEM (FEI QUANTA 200F Field Emission Gun) coupled to an EDAX detector for chemical analysis at 20 kV in low vacuum (0.9 mbar). Raman micro-spectrometry (Jobin Yvon LabRam HR800, $\lambda=632.82$ nm) was also carried out to identify the different oxide phases.

3. Results

3.1 Effect of the preoxidation time of the Ni powder

Fig. 3 shows the cross-section of the preoxidized nickel particles. The Raman spectra of Fig. 4 clearly demonstrate the unique formation of NiO on all particles at different oxidation times at 700°C [21]. The smaller nickel particles (Ni-2) present thicker oxide scales on their surface although the oxidation time is shorter (15 and 40 min) than for the coarse particles (1 and 4 h). Some of the grain boundaries of the coarse particles (Ni-1) are also oxidized. At increased magnifications (see inset in Fig. 3), the surface of Ni-1 exhibits a duplex scale (platelet and compact) after 1 h but the oxide is thicker and porous after 4 h of oxidation. It thus appears that the oxides get thicker with increasing time and number of cycles of oxidation. However, the thickness of the oxide layer varies among the particles (0.3 to 3 μm for 1 h and 1 to 5 μm for 4 \times 1 h). Additional characterization of the coverage with NiO as a function of particle size was performed with "Image J" software (Fig. 5). It can be observed that the smaller the particles, the greater the oxidation. Also, the dependence of oxidation with the particle size decreases with increasing the number of oxidation cycles. Moreover, sintering of the particles caused by oxide growth is observed for all the oxidation times and particle sizes, in particular for the smallest ones (Ni-2). This indicates that the crushing between oxidation cycles was effective in avoiding sintering. In addition, the large particles seem to break along the oxidized grain boundaries and thus form smaller particles upon the repetitive crushing.

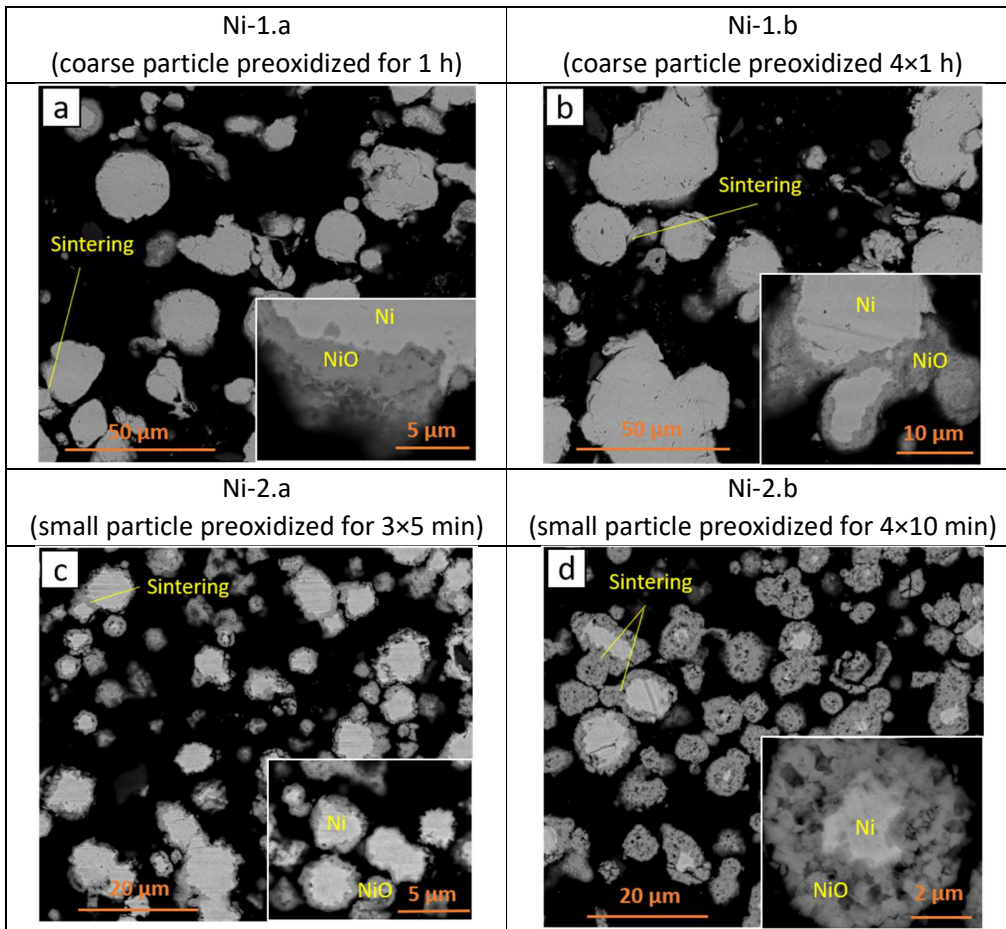


Fig.3: SEM (BSE mode) cross-section images on the coarse (Ni-1.a & Ni-1.b) and small (Ni-2.a & Ni-2.b) preoxidized Ni particles at 700°C in air for different times.

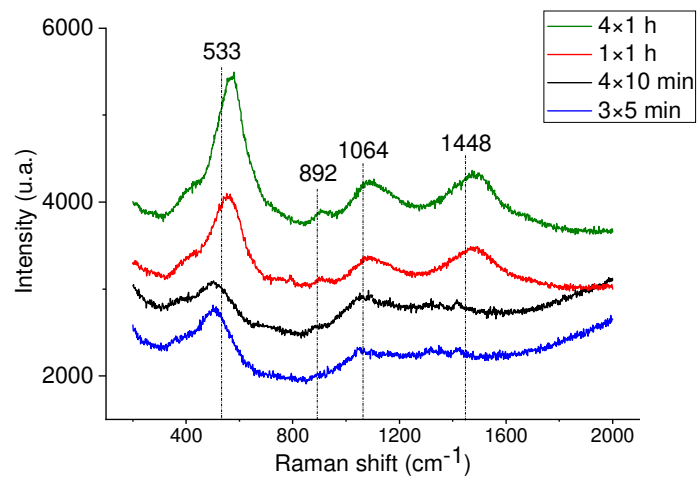


Fig. 4: Raman spectra of the oxides formed on the coarse (Ni-1) and small (Ni-2) particles after oxidation at 700°C in air for different times [21].

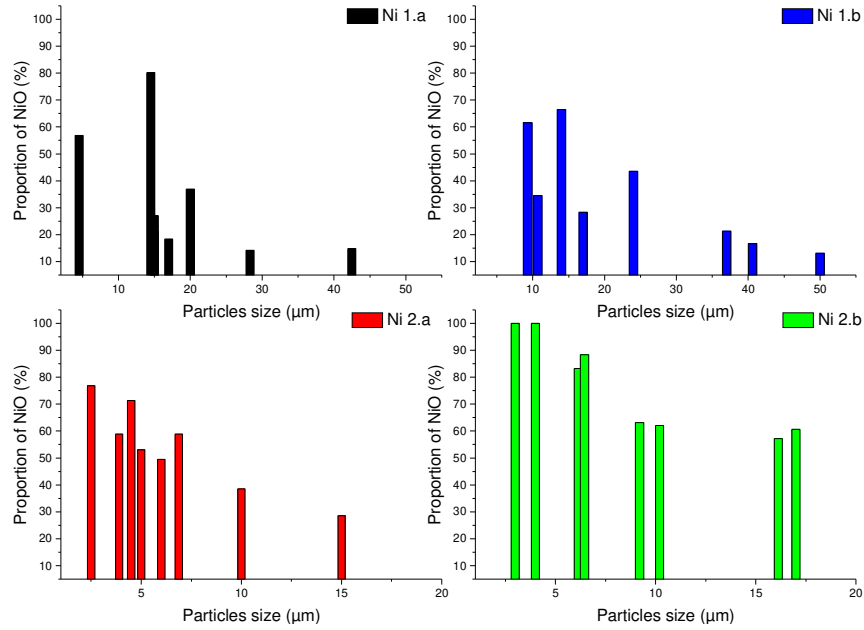


Fig. 5: Area proportion of NiO ($S_{NiO}/S_{Ni} \times 100$) as a function of particle size on the coarse (Ni-1.a & Ni-1.b) and small (Ni-2.a & Ni-2.b) preoxidized Ni particles.

3.2 Reactivity of Al-Ni_{ox} microparticles

Differential scanning calorimetry

The DSC results of the reference powders (Al; metallic Ni-1 and Ni-2; preoxidized Ni-1 and Ni-2) heated at 25°C/min till 1300°C are shown in Fig. 6. The data are summarized in Table 2. Coarse Ni (Ni-1) undergoes an event starting at 346°C that corresponds to the Curie temperature (358°C) [22]. In contrast, the same thermal event is more energetic and starts and finishes at a larger temperature interval when the particles are small (Ni-2). For Al, the onset and the maximum melting temperatures also differ (665 and 677°C for, respectively, the 2 and 25°C/min heating rates) but the overall endotherm is relatively similar. The differences with respect the theoretical melting temperature (660.5°C [23]) can be thus ascribed to the different heating rates [24] that change the manner heat is absorbed.

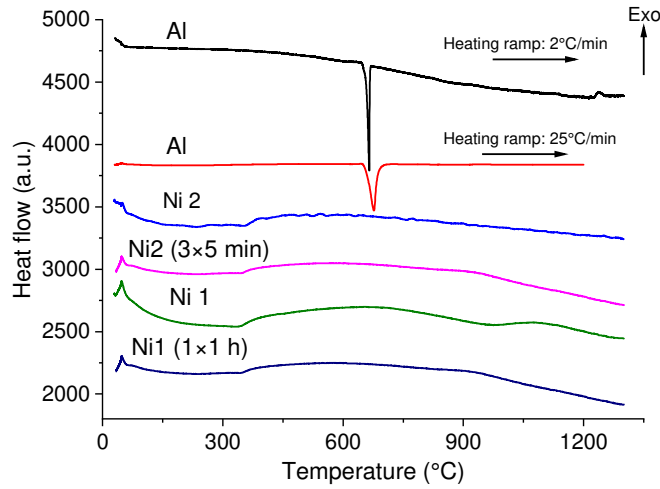


Fig. 6: DSC thermograms for the reference powders (Al, Ni and Ni oxidized) upon heating at 2 and 25°C/min till 1300°C in Ar.

Table 2: Thermal data of the effects observed for the reference powders (Al, Ni and Ni oxidized) upon heating at 2 and 25°C/min till 1300°C in Ar.

Transformation	Ni-1 (coarse particles)			Ni-2 (small particles)		
	T_{\max} (°C)	ΔT (°C)	ΔH (J g ⁻¹)	T_{\max} (°C)	ΔT (°C)	ΔH (J g ⁻¹)
Curie temperature	654	346-950	-81	616	250-1300	-166
	Ni-1.a (coarse preoxidized particles: 1 h)			Ni-2.a (small preoxidized particles: 3x5 min)		
Curie temperature	593	352-901	-105	612	387-1300	-156
	Al-2°C/min			Al-25°C/min		
Melting point	665	645-671	362	677	658-686	385

In the mixed Al + Ni powders, the first exothermic peak at $620 \pm 2^\circ\text{C}$ (label 1 in Fig. 7) is most likely related to a solid-state reaction between Al and NiO [25, 26]. This peak is followed by an endothermic one at $671 \pm 6^\circ\text{C}$, which corresponds to the melting point of Al (label 2 in Fig. 7) [23]. For the coarse oxidized particles (Ni-1), the reaction between Al and Ni occurs at $852 \pm 14^\circ\text{C}$ (label 3 in Fig. 7) and forms Ni_xAl_y intermetallic compounds [27]. Right after, a last exothermic peak (label 4 in Fig. 7) starting above 1000°C can be related to the stabilization of the NiAl intermetallic compound and to the transformation of metastable $\gamma\text{-Al}_2\text{O}_3$ into stable $\alpha\text{-Al}_2\text{O}_3$ [25, 27]. Interestingly, the maximum temperature for NiAl formation is lower in the least preoxidized coarse particles than the ones oxidized for longer times (4x1 h).

For the small preoxidized particles (Ni-2), the same reactions occur until 750°C (Fig. 7, Table 3). However, a clear separation between NiAl and Al_2O_3 cannot be made at higher temperatures because the phenomena are now significantly exothermic. Further, the least oxidized particles (3x5 min) do not

undergo a subsequent transformation of NiAl like the one observed in the preoxidized 4×10 min + Al mixtures.

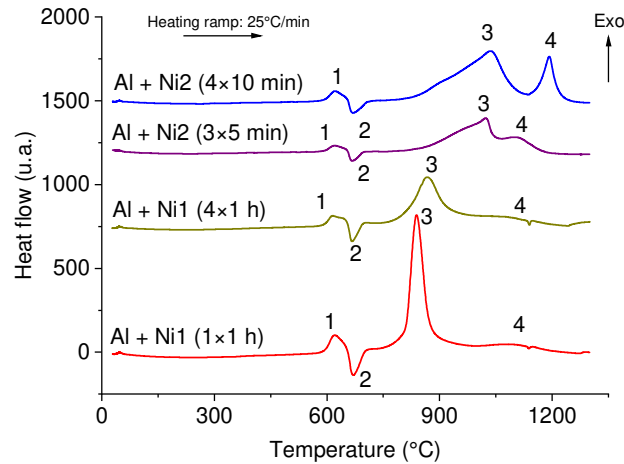


Fig. 7: DSC thermograms of the mixtures of Al with the different Ni particles upon heating 25°C/min till 1300°C in Ar.

Table 3: Thermal data and potential transformations in the mixtures of Al with the different Ni particles.

	T_{\max} (°C)	ΔT (°C)	ΔH (J g ⁻¹)	T_{\max} (°C)	ΔT (°C)	ΔH (J g ⁻¹)
Transformation	Al + Ni-1.a (coarse oxidized Ni particles: 1 h)			Al + Ni-1.b (coarse oxidized Ni particles: 4×1 h)		
NiO reduction	620	526-656	-73	618	540-656	-78
Al melting	671	656-712	63	669	656-711	69
NiAl formation	838	742-988	-596	867	740-1000	-576
γ -Al ₂ O ₃ → α -Al ₂ O ₃	1095	988-1252	-54	1080	993-1142	-52
	Al + Ni-2.a (small oxidized Ni particles: 3×5 min)			Al + Ni-2.b (small oxidized Ni particles: 4×10 min)		
NiO reduction	621	555-655	-66	621	551-655	-72
Al melting	668	655-724	61	670	655-727	81
NiAl formation and γ -Al ₂ O ₃ → α -Al ₂ O ₃	1023	754-1244	-1457	1036	742-1136	-1290
NiAl formation	---	---	---	1192	1136-1272	-314

Microstructural development

The microstructures and the composition of the mixed powders obtained at 750, 1000 and 1300°C are shown in Fig. 8 and Fig. 9. These temperatures correspond to the main exothermic reactions observed in the DSC curves of Fig. 7 (peaks 1, 3 and 4).

In the coarse Ni particles (Ni-1.a and Ni-1.b), all the NiO formed by preoxidation is consumed by the aluminothermic reaction at 671±6°C. As a result, the particles present a homogeneous composition of about 30Al-70Ni (at %) (Figs. 8.a and 8.b). At 1000°C, quite similar concentration gradients of Al and Ni between the core and the external areas are observed in Ni1.a and Ni1.b (labels 1 to 4 in Figs. 8.c and 8.d). Concentrations of Al and Ni of 21-79; 37-63; 48-52 and 58-42 at % are respectively retrieved from

the core to the surface. After the full treatment at 1300°C, all the particles show a fully homogenized NiAl phase with 46Al-54Ni (at %). Moreover, cracks and Kirkendall porosity appear.

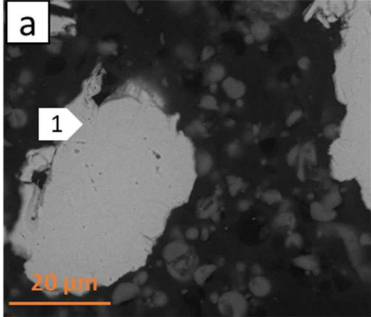
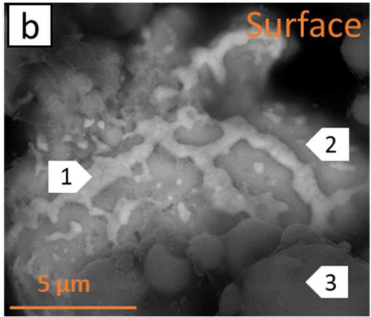
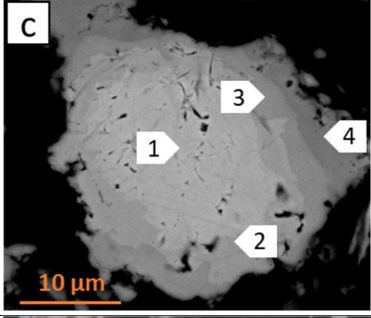
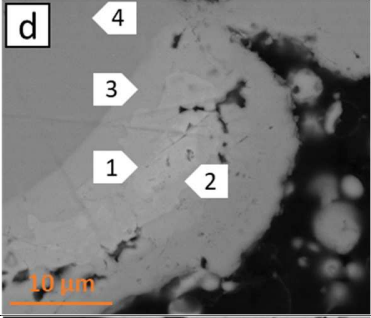
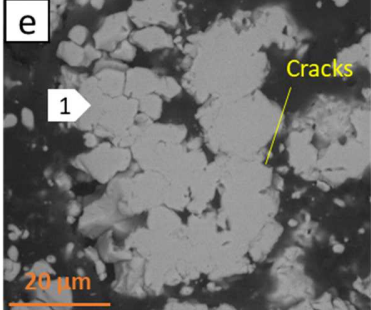
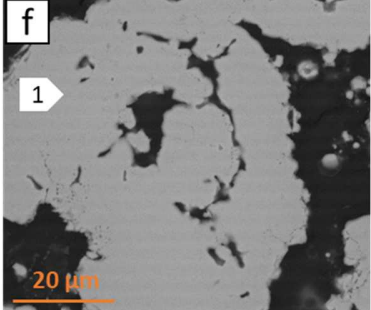
T(°C)	Al + Ni1.a (coarse oxidized Ni particles : 1 h)	Spot	Al (at %)	Ni (at %)	Al + Ni1.b (coarse oxidized Ni particles : 4x1 h)	Spot	Al (at %)	Ni (at %)
750		1	30	70		1	33	67
						2	30	70
						3	94	6
1000		1	21	79		1	27	78
						2	37	63
						3	48	52
						4	58	42
1300		1	46	54		1	46	54

Fig. 8: SEM (BSE mode) of the mixture between Al and coarse Ni preoxidized particles (Ni1.a & Ni2.b) after DSC treatments at 25°C/min for different temperatures.

For the small Ni particles (Ni-2.a and Ni-2.b) preoxidized for 15 and 40 min, NiO is not fully consumed by the aluminothermic reaction before 750°C. The core of the particles presents a homogeneous phase with a composition of Al and Ni, respectively, of 16-84 and 39-61 at % (Figs 9.a and 9.b). Moreover, a high content of Al is found in the oxide when the particles have been preoxidized for 40 min (label 2 in Fig. 9.b) but it was not possible to identify the precise nature of mixed Ni-Al oxide by XRD or Raman spectroscopy. A quasi-stoichiometric NiAl compound has been observed on the outer part of the particles (label 3 Fig. 9.b). For the treatment stopped at 1045°C for Ni-2.a (3x5 min), metallic and partially oxidized particles are observed. The metallic particles are composed of two different zones. One zone has a homogeneous composition of 15Al and 85Ni (at %) (label 1 in Fig. 9.c). Other areas show a gradient of concentration of Al and Ni respectively, 21-79; 32-68 and 38-62 (at %) from the core to the

surface (labels 3 at 5 in Fig. 9.c). Concerning the partially oxidized particles (label 2 in Fig. 9.c), the core presents a homogeneous phase with a composition of 63 Al-37 Ni (at %) while the periphery appears clearly oxidized with Al and Ni.

For the Ni-2.b (4×10 min), two types of partially oxidized particles can be observed. The first type is composed by a metal core with a composition of 11Al-89Ni at % (label 1 in Fig. 9.d), surrounded by an NiO layer which is itself surrounded by a metal layer identical to that of the particle core (view inset Fig. 9.d). The second type of particles is made of a homogeneous phase of 44Al and 56Ni (at %) (label 2 in Fig. 9.d) and interpenetrated alumina. After 1300°C, all the particles show a fully homogenized Ni₃Al phase with 31-68 and 27-73 at % of Al and Ni, respectively (labels 1 in Figs. 9.e and 9.f). Moreover, an aluminum oxide layer can be noticed at the periphery of the particles, as well as some aluminum oxide inclusions inside the particles.

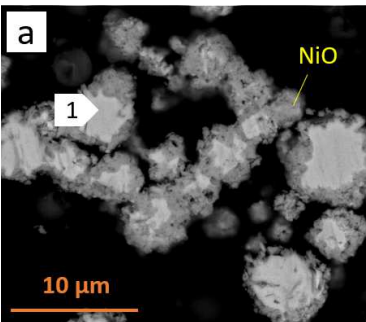
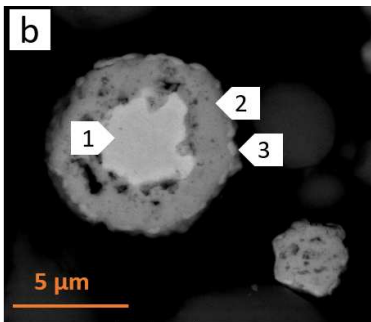
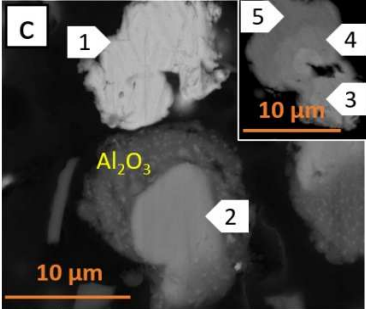
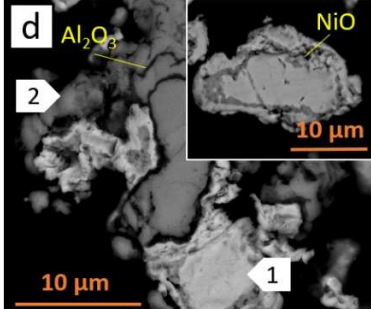
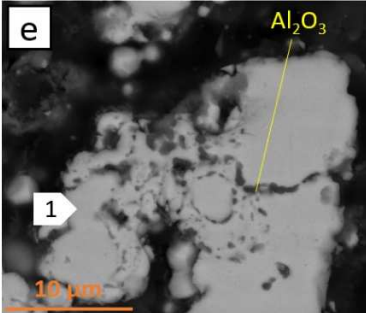
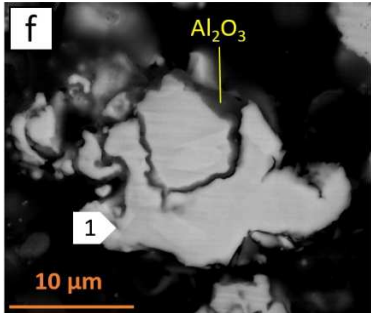
T(°C)	Al + Ni2.a (small oxidized Ni particles : 3x5 min)	Spot	Al (at %)	Ni (at %)	Al + Ni2.a (small oxidized Ni particles : 3x5 min)	Spot	Al (at %)	Ni (at %)
750		1	16	84		1	39	61
						2	43	57
						3	44	56
1045		1	15	85		1	11	89
						2	44	56
						2	63	37
						3	21	79
						4	32	68
1300		1	31	68		1	27	73
						1	27	73

Fig. 9 SEM (BSE mode) of the mixture between Al and small Ni preoxidized particles (Ni-2.a & Ni-2.b) after DSC treatments at 25°C/min for different temperatures.

Therefore in the rest of the study, we will focus on the coarse particles oxidized 4×1 h (Ni-1.b) because the oxide layers are thicker and more homogeneous (Figs. 3 and 5), which should be favorable for the formation of micro-reservoirs. Concerning the small oxidized particles, the particles oxidized 4×10 min (Ni-2.b) will be discarded. Indeed, the oxide layers are conversely too important (Figs. 3 and 5), which would consume a large part of aluminum, likely impeding the formation of an Al-rich intermetallic core rich for the micro-reservoirs.

3.3. Reactivity of preoxidized Ni over pure Al

Differential scanning calorimetry

The DSC results of the different preoxidized Ni particles obtained with two heating ramps (2 and 25°C/min) are shown in Fig. 10 and the thermal data are summarized in Table 4. Reduction of NiO and melting of Al occur at respectively, $620\pm 2^\circ\text{C}$ and $670\pm 2^\circ\text{C}$. For the two heating rates applied to the coarse particles, and for the heating rate of 25°C/min applied to the small ones, many peaks (label 3 in Fig. 10) appear at temperatures ranging between 750 and 1300°C.

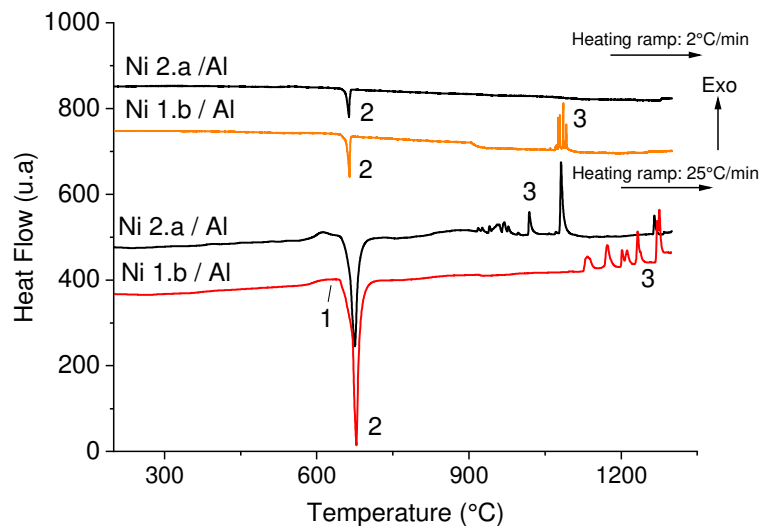


Fig. 10: DSC thermograms of the preoxidized Ni over Al upon heating (2 and 25°C/min) till 1300°C in Ar.

Table 4: Thermal data and the potential transformations in the preoxidized Ni over Al layout

	T _{max} (°C)	ΔT(°C)	ΔH (J g ⁻¹)	T _{max} (°C)	ΔT(°C)	ΔH (J g ⁻¹)
Heating ramp	2°C/min			25°C/min		
Transformation	Ni-1.b / Al			Ni-1.b / Al		
NiO reduction	612	529-649	-50	622	577-648	-9
Al melting	665	649-671	99	678	648-732	104
NiAl formation	1086	1056-1124	-85	1275	1123-1292	-52
	Ni2.a / Al			Ni2.a / Al		
NiO reduction	556	511-549	-76	612	560-648	-14
Al melting	663	649-670	108	675	648-766	95
Ni ₃ Al and NiAl formation $\gamma\text{-Al}_2\text{O}_3 \rightarrow \alpha\text{-Al}_2\text{O}_3$	---	---	---	1081	757-1300	-137

Microstructural development

The microstructure and composition of the layout “preoxidized Ni over Al” heated in Ar following different temperature ramps (2 and 25°C/min) till 1300°C are respectively shown in Figs. 11 and 12. The crucible can be divided into three main sections from the top to the bottom. A summarized description of these different sections is given in Table 5.

The top of the crucibles coincides with the area where the preoxidized Ni particles did not react with Al. No noticeable difference can be observed between the samples (Figs 11.c and 11.d) except for the small oxidized particles for which the recrystallization of the NiO grains occurred forming compact faceted grains (Figs 12.c and 12.d).

The central section of the crucible corresponds to the interface area between preoxidized Ni and Al particles. This zone is composed of different layers of nickel, intermetallic compounds and alumina. The coarse Ni particles form a compact Ni-rich NiAl phase when heated at 25°C/min (label 1, Fig. 11.e). Underneath, an Al-rich NiAl phase with Al₂O₃ segregated at the grain boundaries occurs (label 2 on Fig. 11.e). In between, many pores can be observed. The Al content increases further to the bottom (label 3 on Fig. 11e). For a heating ramp of 2°C/min (Fig. 11.f), the NiAl compounds are also observed but the Al₂O₃ appears more segregated in the Ni-rich NiAl than in the Al-rich counterpart. Further, the interface is not homogeneous and displays cracks rather than pores. Ni/Al₂O₃/Ni-rich NiAl/Al-rich NiAl are distributed on one side and Ni/Al₂O₃ Al-rich NiAl on the other but this can be due to the evolution of the solid powders upon melting.

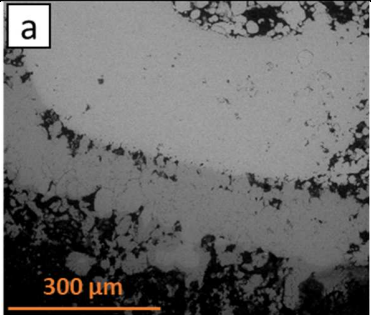
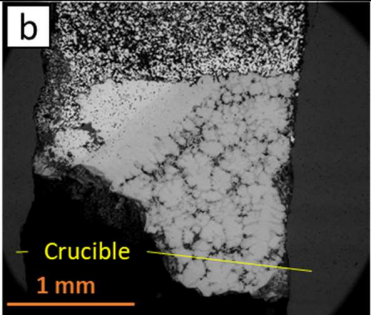
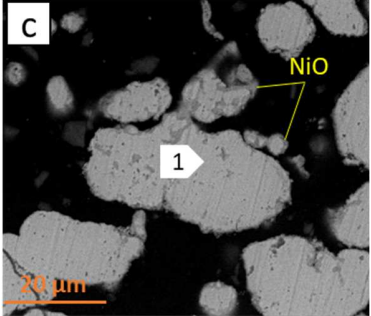
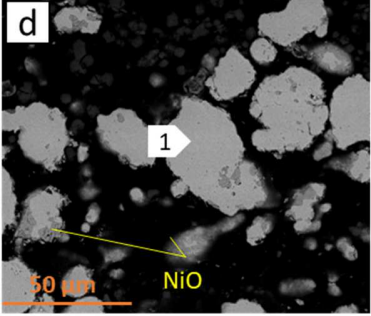
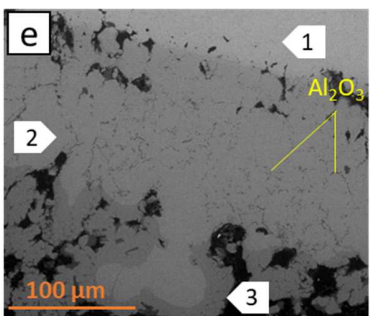
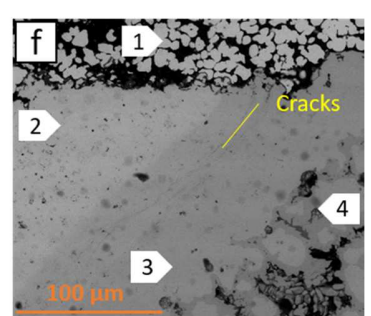
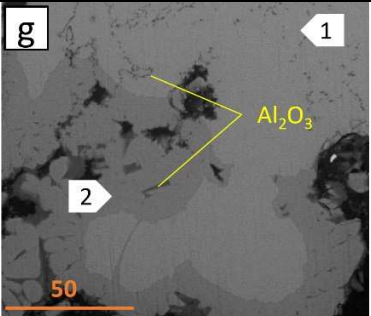
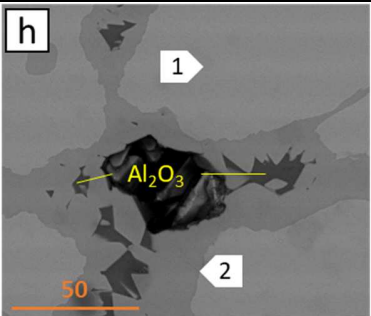
	Heating ramp : 25°C/min			Heating ramp : 2°C/min		
	Spot	Al (at %)	Ni (at %)	Spot	Al (at %)	Ni (at %)
Overview						
Top						
Center (interface between Ni1.b and Al)						
	1	33	67	1	8	92
	2	54	46	2	36	64
	3	62	38	3	56	46
Bottom						
	1	54	46	1	60	40
	2	62	38	2	71	29

Fig. 11: SEM (BSE mode) cross-sections of the layout 2 with coarse preoxidized Ni particles (Ni-1.b over Al after DSC treatments at 25 and 2°C/min. (a) and (b) overview; (c) and (d) top; (e) and (f) center; (g) and (h) bottom of the crucible.

The small Ni particles form Ni₃Al (label 1 on Fig. 12.e) and Ni-rich NiAl (label 2 on Fig. 12.e) when heated at 25°C/min. The Ni-rich NiAl exhibits two different microstructures whereby one is compact and contains Al₂O₃ at the grain boundaries and the other is “porous” and contains Ni-rich NiAl grains trapped in Al₂O₃. At the reduced heating ramp of 2°C/min, clusters of Ni grains (label 1 on Fig. 12.f) and Ni-rich

NiAl (label 2 on Fig. 12.e) can be also observed. The interfaces between these clusters are composed by Al_2O_3 .

For the bottom of the crucibles, there is barely any significant difference between the heating ramps of 25 and 2°C/min. In contrast, the compounds formed differ between the coarse and small Ni particles. Indeed, Al-rich NiAl particles (label 1 in Fig. 11.g) surrounded by Al_3Ni_2 and simultaneous Al_2O_3 formation (label 2 in Fig. 11.g) are developed from the coarse particles. In contrast, the small Ni particles develop both the Ni-rich and the Al-rich NiAl compounds (labels 1 and 2, respectively in Fig. 12.g).

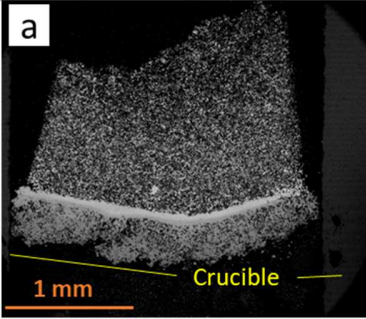
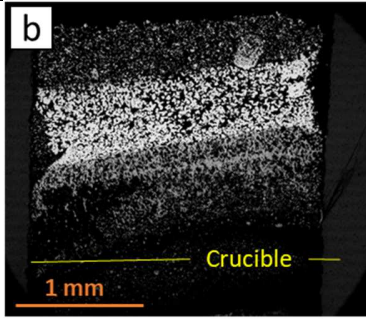
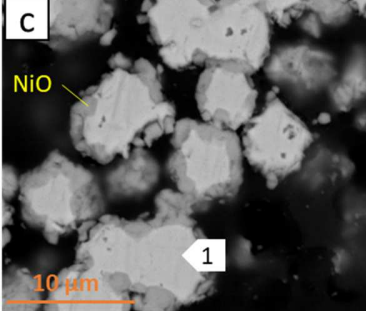
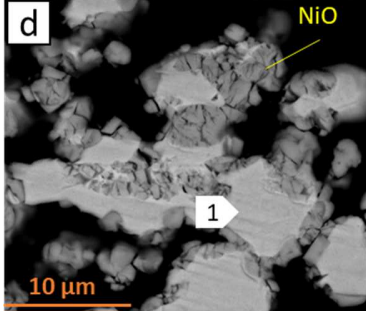
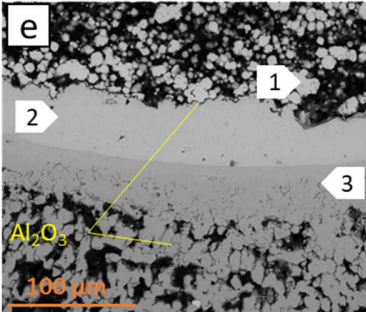
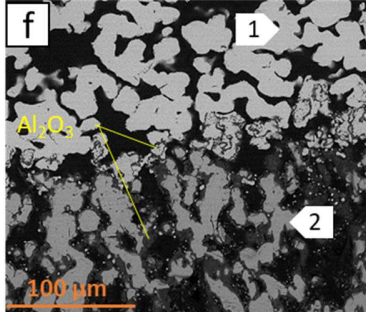
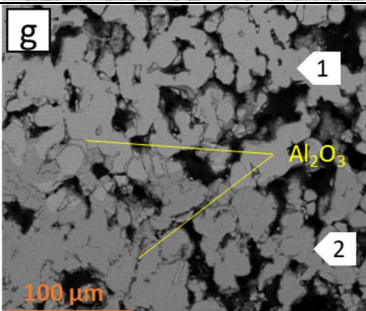
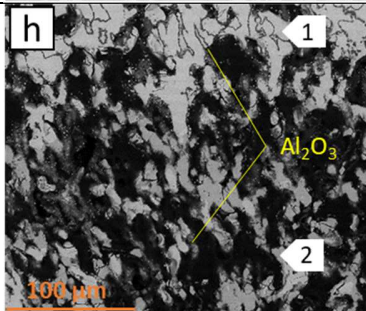
	Heating ramp : 25°C/min	Spot	Al (at %)	Ni (at %)	Heating ramp : 2°C/min	Spot	Al (at %)	Ni (at %)
Overview								
Top		1	1	99		1	1	99
Center (interface between Ni 2.a and Al)		1	6	94		1	4	96
		2	25	75		2	37	63
		3	41	59				
Bottom		1	46	54		1	60	40
		2	60	40		2	71	29

Fig. 12: SEM (BSE mode) cross-sections of the layout 2 with small preoxidized Ni particles (Ni-2.a over Al) after DSC treatments at 25 and 2°C/min. (a) and (b) overview; (c) and (d) top; (e) and (f) center; (g) and (h) bottom of the crucible. Heat treatment (cross-section)

Table 5: Summary of the different zones observed metallographically

Heating ramp	25°C/min		2°C/min	
Particles	Ni-1.a / Al	Ni-2.a / Al	Ni-1.b / Al	Ni-2.a / Al
Zone 1 (top)	Ni particles with NiO	Ni particles with NiO recrystallized	Same as Ni 1.a at 25°C/min	Same as Ni 2.a at 25°C/min
Zone 2 (center)	-Ni particles (10 at % Al) -NiAl (Ni rich) -NiAl (Al rich) with Al ₂ O ₃ grain boundaries	- Ni particles with NiO Interface of Al ₂ O ₃ -Ni ₃ Al -NiAl (Ni rich) with grain boundaries of Al ₂ O ₃	Same as 25°C/min	- Ni particles with NiO -Interface of Al ₂ O ₃ -cluster of NiAl particles with grain boundaries of Al ₂ O ₃
Zone 3 (bottom)	-grains with a NiAl core and Al ₃ Ni ₂ at the edge + Al ₂ O ₃ in grain Al ₃ Ni ₂	- cluster of NiAl (Al rich) particles with grain boundaries of Al ₂ O ₃ -interface of Al ₂ O ₃ - cluster of Al ₃ Ni ₂ particles with grain boundaries of Al ₂ O ₃	Same as Ni 1.a zone 25°C/min but more developed	Same as Ni 2.a 25°C/min

4. Discussion

4.1 Effect of the preoxidation time

Two different Ni powders were oxidized at 700°C under air. The coarse particles (Ni-1) were crushed every hour to avoid the formation of different NiO morphologies and sintering of the oxidized powders. Indeed, porous equiaxial and duplex layer (equiaxial and columnar oxides) forms at the periphery of the Ni coarse particles during oxidation (Fig. 3.a). According to the works of Peraldi et al., a porous NiO scale forms at 700°C for short times [19, 20]. With increasing the oxidation time to 3 h, a duplex scale grows with the porous and equiaxed layer surmounted by columnar grains but the thickness remains almost constant (about 1 µm) [19, 20]. In our case, the formation of the duplex layer appears along the first hour of oxidation with oxide thicknesses ranging from 0.3 to 3 µm (Figs. 3.a and 5.a). The existence of these two types of oxide morphologies within the system may be due to the larger active surface of the Ni powders compared to the average grain size (2 mm) of the Ni studied by Peraldi et al. [19, 20]. When the exposure time is extended to 4 h with crushing of the powder every hour, the scale morphology is exclusively porous with thicknesses ranging from 1 to 5 µm (fig 3.b and 5.b). This difference can be due to the stresses generated by the crushing of the particles, which in turn foster nickel and oxygen interdiffusion and/or provoke the spallation of the columnar grains [29]. In addition, the increase in oxidation time brings about the intergranular oxidation of the Ni particles. The action of crushing effectively disassembles the grains and causes the reduction of the grain sizes and the creation of new un-oxidized surfaces.

The greater reactivity of the smaller Ni particles (Ni-2) is due to their greater specific surface. Such a greater reactivity is demonstrated through the oxide thickness that ranges between 0.5 and 2 µm after just 15 min (i.e. 3×5 min) (Fig 5.c) and between 1.5 and 4 µm after 40 min (i.e. 4×10 min) (Fig 5.d) at 700°C. The oxidation of the small particles is so fast that some of them appear completely oxidized (Fig. 3.d). The small particles preoxidized for 40 min were thus consequently discarded as they would not allow the formation of Al-rich Ni_xAl_y cores in the particle by reaction with Al. Similarly, the coarse particles preoxidized for 1 h did not develop sufficiently thick nickel oxide to results in Al₂O₃ shells upon

the aluminothermic reaction. The coarse and small particles preoxidized for, respectively, 4 h (i.e. 4×1 h) and 15 min (i.e. 3×5 min) were then used to study the formation of the $Ni_xAl_y + Al_2O_3$ phases.

4.2 Layout 1- Mixture of preoxidized Ni and Al particles

The DSC of the Al and preoxidized Ni powders show two peaks at temperatures corresponding to the melting of Al and to the Curie temperature of Ni. When these two powders are mixed together and heated, various additional phenomena appear. The first exothermic peak at $620\pm 2^\circ C$ is most likely related to the solid-state aluminothermic reaction given in equation (1) [30]. The heat released upon this highly exothermic reaction causes the melting of Al and the stop of the solid-state aluminothermic reaction. Whereas by solid state or by molten Al, the whole NiO is consumed by Al to form Al_2O_3 and Ni (Figs. 13.b and 13.c). When the temperature exceeds the melting of Al, the dissolution of Ni can readily occur [31, 32]. Ni and Al are thus quickly consumed and form Ni_3Al (eq. 2) (Fig 13. c).



With increasing temperature between 740 and $1000^\circ C$, further Al inward diffusion occurs and the coarse Ni particles thus develop a concentration gradient between Ni at the core, the intermediate layer of Ni_3Al and the external layer of NiAl (Fig. 13.c). The formation of NiAl is accompanied of a strong exothermic peak shown in Fig. 7 following equation (3) [18]:



The residual Ni is fully transformed with the subsequent heating till $1300^\circ C$. The final microstructure is made of clusters of NiAl particles with many cracks (Fig. 13.d). In contrast, no alumina resulting from the aluminothermic reaction could be detected under the SEM, probably because it is either too thin and/or it came up to the surface given its much lower density than that of the Ni-Al intermetallic compounds.

For the small particles, the exothermic peak at $620^\circ C$ associated with the NiO reduction is also observed but the energy released is lower than with the coarse particles. As a result, a large amount of the NiO grown on the small Ni particles has not reacted yet at about $656^\circ C$ (Fig. 13.f). Between 750 and $1000^\circ C$, the exothermal reaction can be associated with the solid-liquid reduction reaction that brings about an exothermic reaction (Fig. 7). At this range of temperature three types of particles are formed: NiAl/ Al_2O_3 , Ni/ Ni_3Al /NiAl and Ni/NiO/Ni multi-layered microstructures (Fig. 13.g). For the first one, the Ni formed the periphery of the surface is the result of the aluminothermic reaction. These features would imply that the reaction is controlled by the solid-state diffusion of species through the products layers because of the incomplete dissolution of NiO. For the second and the third ones, all the NiO is consumed to form Ni and Al_2O_3 . Moreover, for the third case of Ni(NiO)Ni particles, the Al_2O_3 was expelled.

The full consumption of NiO, Ni and Al at $1050^\circ C$ results in Ni_3Al and Al_2O_3 and the metastable $\gamma-Al_2O_3$ transforms into the stable $\alpha-Al_2O_3$ that releases heat (Fig. 7) [24,33]. Moreover, isolated alumina particles can also be found inside the particles of Ni_3Al .

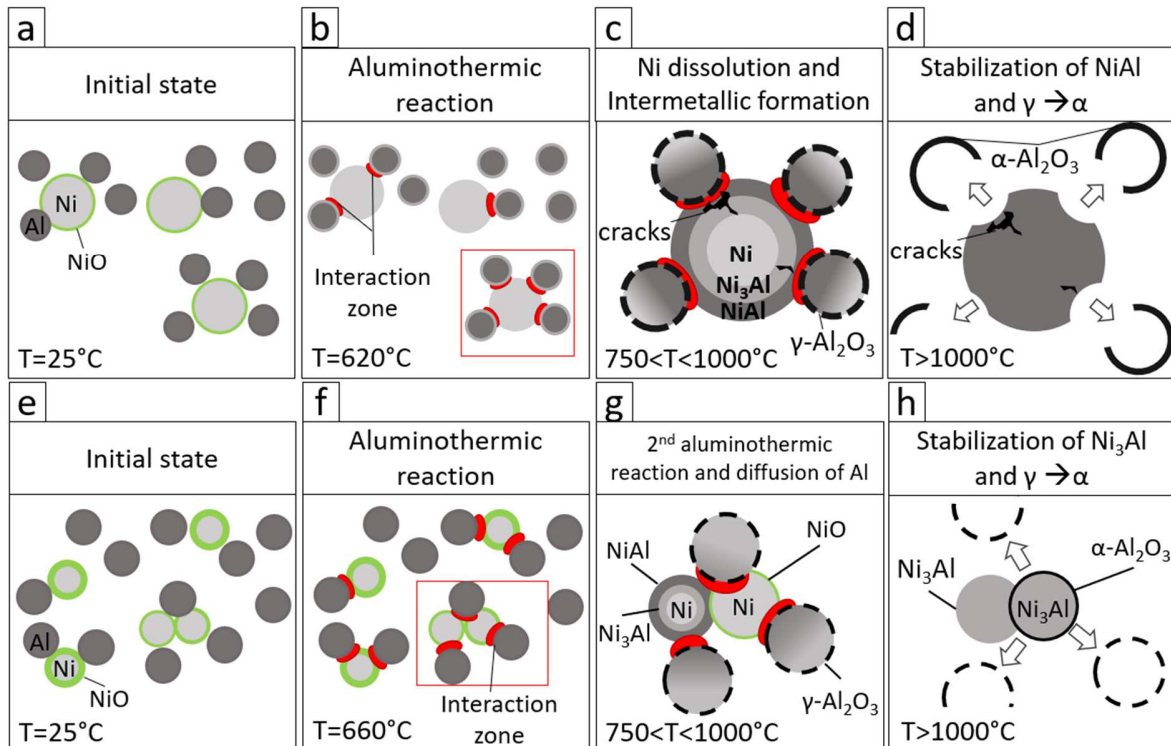


Fig. 13: Schematic model of NiO reduction and formation of intermetallic particles for a mixture of (a-d) coarse preoxidized Ni (4h) and Al and (e-h) small preoxidized (15 min) Ni and Al heated at $25^{\circ}\text{C}/\text{min}$.

4.3 Layout 2- preoxidized Ni powders over the Al particles

The comparison of the results obtained with the mixed particles with that for the layout “preoxidized Ni over Al” clearly points out the tremendous impact of the contact between the reactive particles. Indeed, for the same particle size, the melting enthalpy of Al is much lower with the mixed powders ($\sim 65 \text{ J g}^{-1}$) than with the double layer configuration ($\sim 100 \text{ J g}^{-1}$). Therefore, the greater contact area between Al and NiO results in the formation of more Al_2O_3 absorbing heat and hampering melting of Al. In contrast, when the preoxidized Ni powder is deposited over the Al particles, a front of reactions and of heat propagates from the interface, resulting in different compounds and microstructures.

In this latter configuration (Figs. 14.a and 15.a), the influence of the heating rate appears negligible. Indeed, the DSC curves present the same reaction peaks (within a couple of degrees of difference) and the SEM images exhibit similar zones. However, it has been noted that the extent of the Al-rich areas is greater than that of the Ni-rich area when a slow heating rate ($2^{\circ}\text{C}/\text{min}$) has been applied and vice-versa. This can be related to the fact that diffusion of aluminum is favored below 1000°C [34] (inward diffusion) while the outward diffusion of Ni is promoted above 1000°C [34]. The system therefore spends a longer time at low temperature with slow heating rates.

When the coarse preoxidized Ni particles are heated till 550°C , the solid/solid aluminothermic reaction begins [24]. The external NiO is reduced by Al, bringing about the formation of alumina and of nickel (Fig. 14.b). The resulting particles close to the interface (between Al and NiO particles) are then exposed to the flux of Al, which in turn allows the formation of intermetallic compounds (Ni₃Al and NiAl)

successively towards the core (Fig. 14.b). This stage progressively continues along the crucible until the onset of Al melting is reached ($645\pm 1^\circ\text{C}$). Part of this molten aluminum may be transported upwards by capillarity between the nickel particles. Therefore, the nickel particles get embedded in the molten aluminum (Fig. 14.c). Moreover, the melting of aluminum induces a preferential dissolution of Ni at the grain boundaries and the subsequent formation of cracks, either by shrinkage upon quenching or through the formation of denser phases. Beyond 750°C , aluminum keeps on diffusing through the Ni particles. Therefore, the Ni_xAl_y intermetallics get progressively richer in Al at the expense of Ni-rich Ni_xAl_y . In addition, the grains of the newly formed intermetallic phases grow during this stage causing the disappearance of porosity. The molten aluminum between these grains will be gradually “absorbed” by the Ni particles leaving behind alumina trapped between the grains (Fig. 14.c).

Between 1000 and 1300°C , the microstructure barely evolves while the composition slightly changes due to favored nickel diffusion. This results in Al-rich and Ni-rich NiAl compounds (Fig. 14.d). Quenching to room temperature provokes solidification of molten Al and the segregation of Al_3Ni_2 between the grains of Al-rich NiAl (Fig. 14.d).

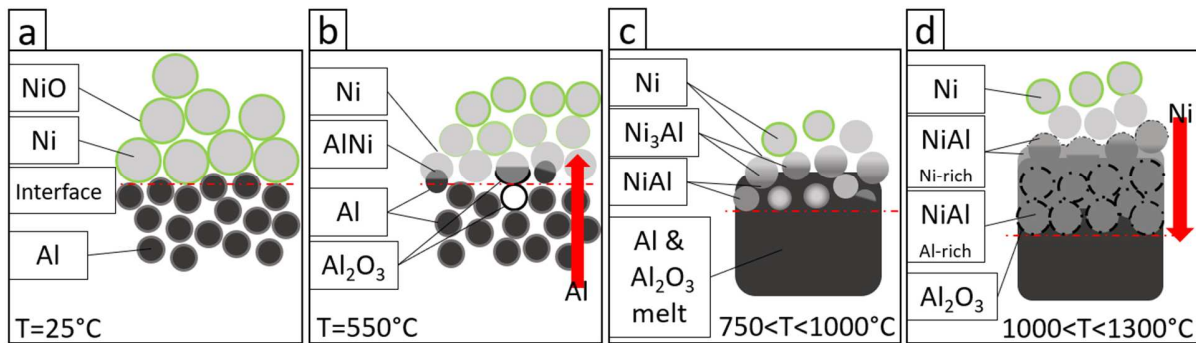


Fig. 14: Schematic drawings of the aluminothermic reduction and reactions between the coarse preoxidized Ni over Al particles (double layer configuration) heated at $25^\circ\text{C}/\text{min}$.

For the small particles the effect of the heating rate is very significant as demonstrated by the different DSC peaks (Fig. 10) and SEM microstructures at the center of the crucibles (Fig. 12). These differences can result from the preoxidation of the powders whereby the oxide growth at 700°C is ruled by the faster diffusion rate of the Ni^{2+} ions than that of the O^{2-} ions. As a consequence, pores and cavities are generated at the oxide/metal interface [35]. Further the particles are subjected to intermediate air quenching and crushing (3×15 min), which induce stress in the oxide and in the metallic Ni particle. These phenomena are enhanced on the small particles vs. the coarse ones because of their greater oxide thickness and less spherical morphology. Overall, the small particles become more reactive than the coarse ones.

When the temperature of 550°C is reached, the solid/solid aluminothermic reaction begins [27], NiO and Al react at the interface of the preoxidized Ni particles (Fig. 15.b). As opposed to the coarse particles, the thickness of the oxide layer is now quite significant and the aluminothermic reaction is thus momentarily superseded by the onset of the Al melting at $648\pm 1^\circ\text{C}$. Molten Al flows upwardly by capillarity between the Ni preoxidized particles NiO grains causing the entrapment of nickel particles in the molten Al and the enrichment of the NiO in Al (Fig. 15.c). Beyond 750°C , the second aluminothermic reaction (liquid/solid) begins. The remainder of the NiO near the interface is thus finally converted into an

adherent Al_2O_3 (Fig. 15.c). Simultaneously, the NiO “barrier” over the Ni particles is transformed in Al_2O_3 creating cracks, the Ni core is directly exposed to the molten Al (Fig. 15.c). The greater amount of alumina formed at this stage aggregates around the particles and prevents their sintering. As a result, clusters of intermetallic compounds with a lot of porosity are obtained (Fig. 15.c).

When the temperature reaches 950°C , a third exothermic peak appears when heating at $25^\circ\text{C}/\text{min}$ (Fig. 10 peak labeled 3'). This peak results from the transformation of the Ni phase into Ni_3Al and NiAl but the reaction does not take place continuously. This reaction can be explained by the difference in the thermal expansion coefficient between Ni and NiO and the potential residual stress and cavities that cause cracking and spallation of the NiO layer. Therefore, Al becomes free to react with Ni and form Ni_3Al and NiAl . The NiO expelled continue its reduction in the molten Al to form Al_2O_3 that gets trapped between the grains of the intermetallic compounds as they grow. This step will be repeated until the intermetallic layer thickens enough to hamper the arrival of Al. The heat produced during this stage and the very low amount of trapped oxide do not prevent the sintering of the particles to each other to form a compact structure. The Ni_3Al layer will subsequently enrich with Al to form NiAl (Fig. 15.d).

In contrast, cracking and spallation of NiO do not occur when heating at $2^\circ\text{C}/\text{min}$. Therefore, when the temperature reaches 750°C , the solid/liquid aluminothermic reaction occurs and the remainder of the NiO near the interface is finally converted into an adherent Al_2O_3 . Simultaneously, the NiO “barrier” over the Ni particles being reduced, the Ni core can now react directly with the molten Al (Fig. 15.c). The greater amount of alumina formed at this stage aggregates around the particles and prevent their sintering. As a result, clusters of intermetallic compounds with significant porosity are obtained (Fig. 15.c)

Deeper in the crucible and irrespective of the heating rate, clusters of Al_3Ni_2 and Al_3Ni are formed upon cooling (Fig. 15.d). At the surface of these clusters, almost no Al_2O_3 was observed, which suggests that Al_2O_3 either dissolves and/or that is transported to the surface of the melt given its lower density than the intermetallic compounds.

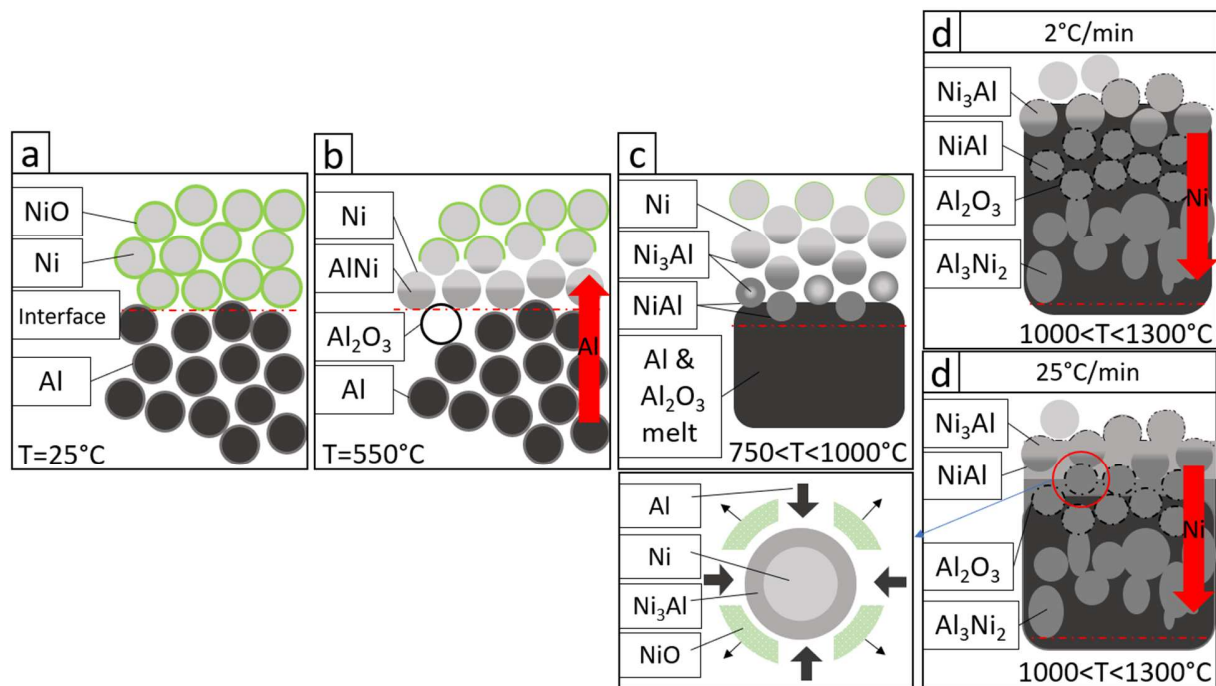


Fig. 15: Schematic drawings of the aluminothermic reduction and reactions between the small preoxidized Ni on Al (double layer configuration) heated at 2 and 25°C/min

5. Conclusion

The reaction process of a $Ni_xAl_y-Al_2O_3$ phases via thermite reaction of preoxidized Ni particles and aluminum particles was investigated by DSC and metallographic observations. It was found that different intermediate phases formed during heating of the powder mixtures. Metallic Ni formed first at around 600°C, followed by the formation of Ni_3Al and NiAl and a temperature increase. After 1300°C, the coarse preoxidized Ni powders formed a cluster of NiAl particles while the small preoxidized Ni particles resulted in a cluster of interpenetrated Ni_3Al and Al_2O_3 . The formation of Al_2O_3 is believed to result from a three-stage process. Initially, a small amount of Al_2O_3 was produced by the reduction of NiO with solid Al. Then, Al_2O_3 particles formed by the reduction of NiO with liquid Al. Finally, Al_2O_3 developed by the solid-state displacement reaction between NiO and nickel-aluminides (Al_3Ni , Al_3Ni_2 , NiAl).

When the coarse preoxidized Ni particles lay over the Al ones, a dense structure composed by a Ni-rich NiAl above an Al-rich NiAl was formed. The Al_2O_3 formed by thermite reaction was trapped in the grain boundaries of the Al-rich NiAl. However, the small preoxidized Ni particles grew a dense structure with Ni_3Al above a Ni-rich NiAl and Al_2O_3 trapped in the grain boundaries in some areas and clusters of Al-rich NiAl and Al_3Ni_2 particles surrounded by a thin layer of Al_2O_3 in some other areas.

These results, therefore, suggest that the synthesis of self-regenerating coating could be obtained by e.g. spraying slurries containing mixtures of preoxidized Ni and metal Al or multilayering them onto a substrate. Subsequent heat treatments with relatively fast heating ramps (25°C) till moderate temperatures (~ 750°C) assisted by the aluminothermic reaction between NiO and Al could consolidate the formation of the micro-containers trapped in the coating.

6. References

- [1] G.W. Goward, *Current research on the surface protection of superalloys for gas turbine engines*, JOM 22 (1970) 31–39.
<https://10.1007/BF03355665>.
- [2] J. Stringer, *High-temperature corrosion of superalloys*, Mater. Sci. Technol. 3 (1987) 482–493.
<https://10.1080/02670836.1987.11782259>.
- [3] M.W. Brumm, H.J. Grabke, *The oxidation behaviour of NiAl – I. Phase transformations in the alumina scale during oxidation of NiAl and NiAl-Cr alloys*, Corros. Sci. 33 (1992) 1677–1690.
[https://10.1016/0010-938X\(92\)90002-K](https://10.1016/0010-938X(92)90002-K).
- [4] H.J. Choi, J. Jedlinski B. Yao, Y.H. Sohn, *Transmission electron microscopy observations on the phase composition and microstructure of the oxidation scale grown on as-polished and yttrium-implanted β -NiAl*, Surf. Coat. Technol. 205 (2010) 1206–1210.
<https://10.1016/j.surfcoat.2010.10.034>.
- [5] J.R. Nicholls, *Designing oxidation-resistant coatings*, JOM 52 (2000) 28–35.
<https://10.1007/s11837-000-0112-2>.
- [6] G.W. Goward, D.H. Boone, *Mechanisms of formation of diffusion aluminide coatings on nickel-base superalloys*, Oxid. Met. 3 (1971) 475–495.
<https://10.1007/BF00604047>.
- [7] N. Vialas, D. Monceau, *Effect of Pt and Al content on the long-term high temperature oxidation behavior and interdiffusion of Pt-modified aluminide coating deposited of Ni-base superalloys*, Surf. Coat. Technol. 201 (2006) 3846–3851.
<https://10.1016/j.surfcoat.2006.07.246>.
- [8] Y. Matsumura, M. Fukumoto, S. Hayashi, A. Kasama, I. Iwanaga, R. Tanak, T. Narita, *Oxidation behavior of a Re-base diffusion-barrier/NiAl coating on Nb–5Mo–15W at high temperatures*, Oxid. Met. 61 (2004) 105–124.
<https://10.1023/B:OXID.0000016279.88052.d9>.
- [9] Y. Wang, H. Guo, H. Peng, L. Peng, S. Gong, *Diffusion barrier behaviors of (Ru, Ni) Al/NiAl coatings on Ni-based superalloy substrate*, Intermetallics 19 (2011) 191–195.
<https://10.1016/j.intermet.2010.08.016>.
- [10] T. Narita, *Diffusion barrier coating system concept for high temperature applications*, Canadian Metallurgical Quarterly 50 (2011) 278–290.
<https://10.1179/1879139511Y.0000000014>.
- [11] R.M. German, *Sintering-Theory and Practice*, Wiley Interscience, (1996).
- [12] P. Nieroda, R. Zybała, K.T. Wojciechowski, *Development of the method for the preparation of Mg_2Si by SPS technique*, Am. Inst. Phys. Conf. Proc. 1449 (2012) 199–202.
<https://10.1063/1.4731531>.

- [13] M. Chmielewski, K. Pietrzak, *Processing, microstructure and mechanical properties of Al₂O₃-Cr nanocomposites*, J. Eur. Ceram. Soc. 27 (2007) 1273–1279.
<https://10.1016/j.jeurceramsoc.2006.05.093>.
- [14] E.M. Levin, C. R. Robbins, H.F. McMurdie, *Phase diagrams for ceramists*, American Ceramic Society (1990) 90.
- [15] J.Z. When, S. Ringuette, G. Bohlouli-Zanjani, A. Hu, N.H. Nguyen, J. Persic, C.F. Petre, Y.N. Zhou, *Characterization of thermochemical properties of Al nanoparticles and NiO nanowire composites*, Nanoscale Res. Lett. 8 (2013) 184.
<https://10.1186/1556-276X-8-184>.
- [16] D. Vrel, P. Langlois, E.M. Heian, N. Karnatak, S. Dubois, M.F. Beaufort, *Reactions kinetics and phase segregation in the 3NiO + 2Al → Al₂O₃ Thermite system*, Int. J. Self-Propagating High-Temp. Synth. 12 (2004) 261–270.
- [17] D. Vrel, A. Hendaoui, P. Langlois, S. Dubois, V. Gauthier, B. Cochapin, *SHS reactions in the NiO-Al system: Influence of stoichiometry*, Int. J. Self-Propagating High-Temp. Synth. 16 (2007) 62–69.
<https://10.3103/S1061386207020021>.
- [18] A. Biswas, S.K. Roy, K.R. Gurumurthy, N. Prabhu, S. Banerjee, *A study of self-propagating high-temperature synthesis of NiAl in thermal explosion mode*, Acta Mater. 50 (2002) 757–773.
[https://10.1016/S1359-6454\(01\)00387-1](https://10.1016/S1359-6454(01)00387-1).
- [19] R. Peraldi, D. Monceau, B. Pieraggi, *Correlations between growth kinetics and microstructure for scales formed by high-temperature oxidation of pure nickel, I. Morphologies and Microstructures*, Oxid. Met. 58 (2002) 249–273.
<https://10.1023/A:1020170320020>.
- [20] R. Peraldi, D. Monceau, B. Pieraggi, *Correlations between growth kinetics and microstructure for scales formed by high-temperature oxidation of pure nickel, II. Growth Kinetics*, Oxid. Met. 58 (2002) 275–295.
<https://10.1023/A:1020102604090>.
- [21] N. Mironova-Ulmane, A. Kuzmin, I. Steins, J. Grabis, I. Sildos, M. Pärs, *Raman scattering in nanosized nickel oxide NiO*, J. Phys. Conf. Series 93 (2007).
<https://10.1088/1742-6596/93/1/012039>.
- [22] R. Serway, R. Beichner, W. John, Jr. Jewett, *Physics for Scientists and Engineers*, Forth Worth Saunders College Publishing 2 (2000) 1551.
- [23] H. Okamoto, *Al-Cr (Aluminum-Chromium)*, J. Phase Equilibria Diffus. 29 (2008) 112–113.
<https://10.1007/s11669-007-9225-4>.
- [24] F. Pedraza, M. Mollard, B. Rannou, J. Balmain, B. Bouchaud, G. Bonnet, *Potential thermal barrier coating systems from Al microparticles. Mechanisms of coating formation on pure nickel*, Materials Chemistry and Physics 134 (2012) 700–705.
<https://10.1016/j.matchemphys.2012.03.053>.

- [25] V. Udhayabanu, N. Singh, B.S. Murty, *Mechanical activation of aluminothermic reduction of NiO by high energy ball milling*, J. Alloys Compd. 497 (2010) 142–146.
<https://10.1016/j.jallcom.2010.03.089>.
- [26] H.X. Zhu, R. Abbaschian, *In-situ processing of NiAl-alumina composites by thermite reaction*, Mater. Sci. Eng. 282 (2000) 1–7.
[https://10.1016/S0921-5093\(99\)00788-1](https://10.1016/S0921-5093(99)00788-1).
- [27] D. Padmavardhani, A. Gomer, R. Abbaschian, *Synthesis and microstructural characterization of NiAl-Al₂O₃ functionally gradient composites*, Intermetallics 6 (1998) 229–241.
[https://10.1016/S0966-9795\(97\)00076-9](https://10.1016/S0966-9795(97)00076-9).
- [28] R. Przeliorz, J. Piatkowski, *Application of DSC method in studies on phase transitions of Ni Superalloys*, Archives of Foundry Engineering 17 (2017) 133–136.
<https://10.1515/afe-2017-0144>.
- [29] H.E. Evans, *Stress effects in high temperature oxidation of metals*, International Materials Review 40 (1995) 1–40.
<https://10.1179/imr.1995.40.1.1>.
- [30] A.M. Padhan, M. Sathish, P. Saravanan, *Mechanical activation on aluminothermic reduction and magnetic properties of NiO powders*, J. Phys. Appl. Phys. 50 (2017).
<https://10.1088/1361-6463/aa6cee>.
- [31] B. Bouchaud, B. Rannou, F. Pedraza, *Slurry aluminizing mechanisms of Ni-based superalloys incorporating an electrosynthesized ceria diffusion barrier*, Materials Chemistry and Physics 143 (2013) 416–424.
<https://10.1016/j.matchemphys.2013.09.022>.
- [32] M.C. Galetz, X. Montero, M. Mollard, M. Günthner, F. Pedraza, M. Schütze, *The role of combustion synthesis in the formation of slurry aluminization*, Intermetallics 44 (2014) 8–17.
<https://10.1016/j.intermet.2013.08.002>.
- [33] N. Eisenreich, H. Fietzek, M. del Mar Juez-Lorenzo, V. Kolarik, A. Koleczko, V. Weiser, *On the mechanism of low temperature oxidation for aluminum particles down to the nano-scale*, Propellants, Explosives, Pyrotechnics 29(2004) 137–145.
<https://10.1002/prop.200400045>.
- [34] J.M. Brossard, B. Panicaud, J. Balmain, G. Bonnet, *Modelling of aluminized coating growth on nickel*, Acta Mater. 55 (2007) 6586–6595.
<https://10.1016/j.actamat.2007.08.025>.
- [35] Q. Jeangros, T.W. Hansen, J. B. Wagner, R. E. Dunin-Borkowski, C. Hébert, J. Van Herle, A. Hessler-Wyser, *Oxidation mechanism of nickel particles studied in an environmental transmission electron microscope*, Acta Mat. 67(2014) 362–372
<https://10.1016/j.actamat.2013.12.035>

